JOURNAL OF Applied Polymer SCIENCE

Tailored Dielectric and Mechanical Properties of Noncovalently Functionalized Carbon Nanotube/Poly(styrene-*b*-(ethylene-*co*-butylene)-*b*-styrene) Nanocomposites

Santosh Kumar Yadav,* Sibdas Singha Mahapatra, Jae Whan Cho
Department of Textile Engineering, Konkuk University, Seoul 143-701, Korea
*Present address: Center for Materials Architecturing, Korea Institute of Science and Technology, Seoul 136-791, Korea
Correspondence to: J. W. Cho (E-mail: jwcho@konkuk.ac.kr)

ABSTRACT: The preparation of high-dielectric poly(styrene-*b*-(ethylene-*co*-butylene)-*b*-styrene) (SEBS) composites containing functionalized single-walled carbon nanotubes (f-SWCNTs) noncovalently appended with dibutyltindilaurate are reported herein. Transmission electron microscopy and X-ray photoelectron and Raman spectroscopy confirmed the noncovalent functionalization of the SWCNTs. The SEBS-f-SWCNT composites exhibited enhanced mechanical properties as well as a stable and high dielectric constant of approximately 1000 at 1 Hz with rather low dielectric loss at 2 wt% filler content. The significantly enhanced dielectric property originates from the noncovalent functionalization of the SWCNTs that ensures good dispersion of the f-SWCNTs in the polymer matrix. The f-SWCNTs also acted as a reinforcing filler, thereby enhancing the mechanical properties of the composites. © 2013 Wiley Periodicals, Inc. J. Appl. Polym. Sci. 000: 000–000, 2013

KEYWORDS: composites; nanotubes; graphene and fullerenes; elastomers

Received 24 June 2012; accepted 18 December 2012; published online
DOI: 10.1002/app.38938

INTRODUCTION

Polymer-based composites with highly superior dielectric performance are currently very attractive research topics in the discipline of materials science and have continued to garner attention in recent years.[1] This interest stems from their pertinency in electric devices such as actuators, artificial muscles, capacitors for energy storage, and as high-dielectric constant gate dielectrics for flexible electronics.[2,3] However, the dielectric permittivity of typical polymers is dispiritingly low, and thus much effort has been concentrated on using ceramics, metals, or conducting polymers as dielectric fillers in the polymer matrix to obtain relatively high dielectric permittivity.[4,5] Although a significant quantity (>50 vol %) of filler has been bound in the polymer matrix of these composite structures, these fillers introduce a number of limitations in terms of weight, flexibility, mechanical properties, and huge dielectric loss.[6,7] Thus, enhancement of the dielectric constant of the polymers while retaining their other excellent properties is a key issue.

Carbon nanotubes (CNTs) have attracted tremendous interest due to their extraordinary electrical, thermal, and mechanical properties.[8–10] Additionally, owing to their prominent dielectric constants, they are also attractive fillers for high dielectric constant composites.[11,12] Polymer/CNT composites enable the possiblility of harnessing the extraordinary properties of nanotubes on a macroscopic scale in the construction of stretchable electronics. A genuine problem in fabricating CNT composites is the individual dispersion of the CNT into the host polymeric material and sustaining effective interactions between the nanotubes and the polymer matrix. Individual dispersion of CNT is strongly affected by the high Van der Waals forces of attraction between adjacent tubes and high aspect ratio, which gives rise to the formation of aggregates and inhibits the translation of nanophysical properties to nanocomposites. Various attempts have been made to circumvent these problems, and several methods have so far been reported for the fabrication of polymer–CNT nanocomposites. One of the most promising means of enhancing the dispersion of the CNTs and the interfacial bonding between the CNTs and the polymer matrix is functionalization of the CNTs.[13–15] However, aggressive chemical functionalization at high temperatures induces defects on the CNT surface, thereby altering the electrical properties of the CNTs.[16–18] Lucente-Schultz et al. have reported that when single-walled CNTs (SWCNTs) are aggressively oxidized in a mixture of fuming sulfuric acid (oleum) and nitric acid, the length of the SWCNTs is shortened or cut and the sidewalls are functionalized. The introduced corboxylic group then makes it possible for defects to be created.[19] Noncovalent functionalization of

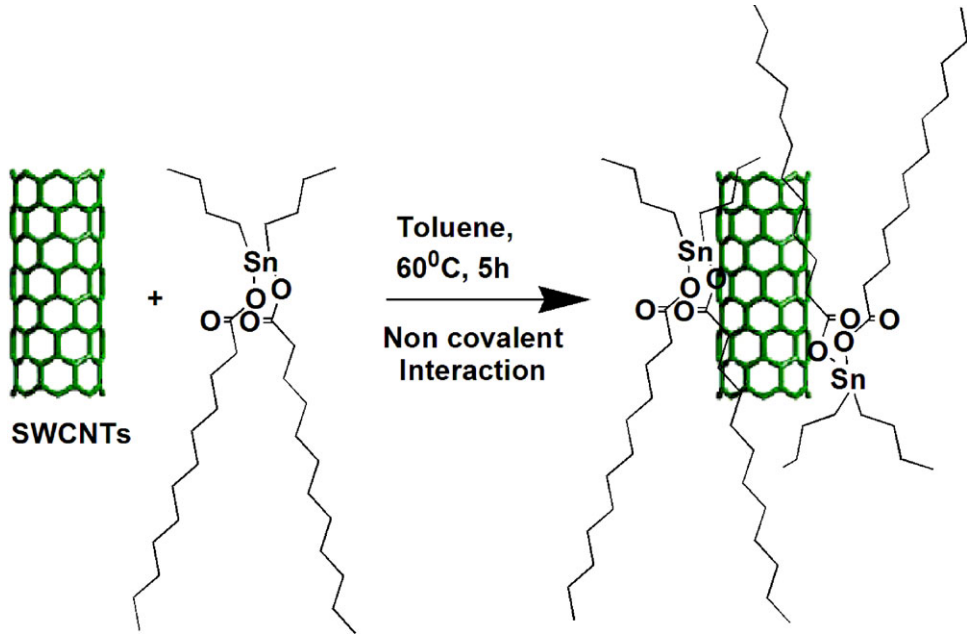

Scheme 1. Strategy for noncovalent functionalization of SWCNTs. [Color figure can be viewed in the online issue, which is available at wileyonlinelibrary.com.]

CNTs is of particular interest because it does not compromise the physical properties of CNTs. Chen et al.[20] have reported a simple and general approach to noncovalent functionalization of the sidewalls of SWCNTs and subsequent immobilization of various biological molecules onto nanotubes with a high degree of control and specificity. Kang et al. have used noncovalent method to modify SWNTs by encapsulating SWNTs within crosslinked and amphiphilic poly(styrene)-*block*-poly(acrylic acid) copolymer micelles. This encapsulation significantly enhanced the dispersion of SWNTs in a wide variety of polar and nonpolar solvents and polymer matrices. Thus, encapsulated SWNTs may be stabilized with respect to typical polymer processing.[21]

We have used the noncovalent functionalization technique for fabrication of a high-dielectric polymer composite. Recently, we have also reported a simple procedure for the fabrication of composites composed of SWCNTs and a hyperbranched polymer having excellent mechanical properties and tunable dielectric permittivity; nevertheless, this method was limited in terms of control of the huge dielectric loss.[3] Dang et al.[22] reported the fabrication of three phase nanocomposites comprising CNTs and $BaTiO_3$ with poly(vinylidene fiuoride) that displayed a large dielectric constant of 900 above a critical filler content; nevertheless, these composites still exibited high dielectric loss. Yang et al. prepared MWCNTs/polypyrrole core-shell nanostructures by an inverse microemulsion polymerization. They could achieve the dielectric constant up to 44 after high loading (10 wt %) of MWCNT/polypyrrole into the polystyrene matrix.[23]

Chen et al.[24] proposed a core-shell structure of multiwalled carbon nanotubes as a filler, in which the outer graphene layer was covalently functionalized to become nonconducting. This composite exhibited a dramatic increase of the dielectric constant, while minimizing the dielectric loss of the CNT–polymer composites.[24]

The approach used in this study involves harnessing the excellent electrical properties of CNTs in the construction of high dielectric polymer composites with low dielectric loss by incorporating noncovalently functionalized SWCNTs into the poly(-styrene-*b*-(ethylene-*co*-butylene)-*b*-styrene) (SEBS) triblock copolymer. Dibutyltindilaurate (DBTDL) has been used as a catalyst and a stabilizer for polymers. DBTDL contains Sn metal in the center; the current approach can thus be considered as a kind of metal doping on the SWCNT surfaces. The utility of SEBS has been well established in the development of multifunctional materials targeting a variety of applications such as actuators, sensors, biomaterials, microcontact printing, and elastomers.[25–28]

EXPERIMENTAL

Materials and Reagents

SWCNTs (Hipco) with diameters and lengths of 0.8–1.2 nm and 1–10 μm, respectively, were purchased from Unidym, Sunnyvale, CA. DBTDL was purchased from Aldrich, Seoul, Korea. Toluene was used after purification by the conventional technique and stored over type 4 Å molecular sieves.

Functionalization of SWCNTs

The noncovalently functionalized SWCNTs (f-SWCNT) were prepared by the following method. First, 500 mg of SWCNTs were dispersed in a flask containing 50 mL of toluene using bath sonication for 10 min at room temperature. Subsequently, 5 mL of DBTDL was added to the flask, and the mixture was heated at 60°C with continuous stirring for 5 h. The resulting product was washed with copious amounts of toluene followed

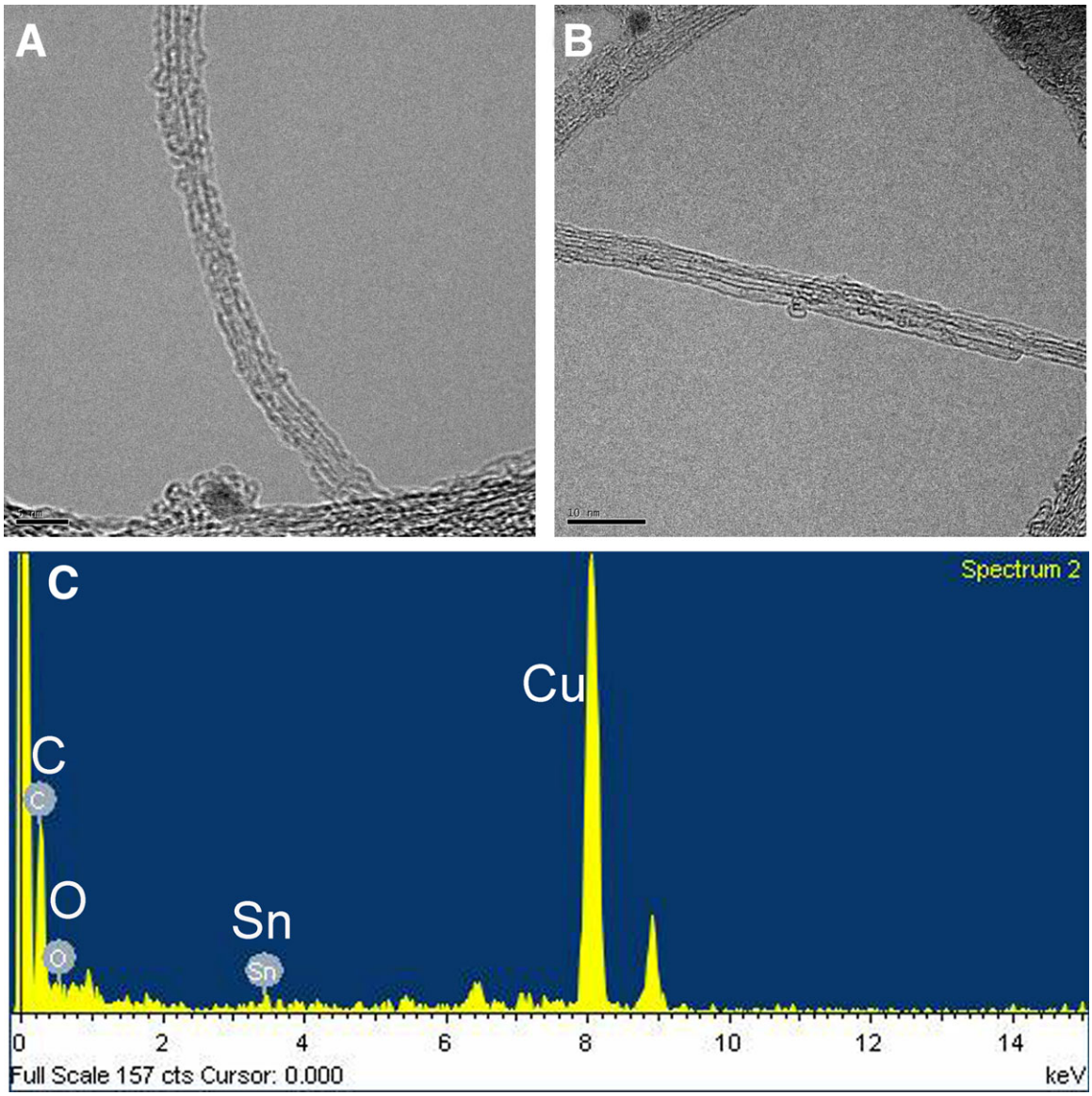

Figure 1. TEM images (A, B), and EDX spectrum (C) of the noncovalently functionalized SWCNTs. [Color figure can be viewed in the online issue, which is available at wileyonlinelibrary.com.]

by acetone to obtain f-SWCNT; the final product was dried at 80°C.

Preparation of SEBS-f-SWCNT Nanocomposites via Solvent Casting

Noncovalently functionalized SWCNT-filled SEBS triblock copolymer films were fabricated according to the following procedure. First, the f-SWCNTs were dispersed in toluene under sonication, while the SEBS was separately dissolved completely in toluene. The combined preparations were subjected to bath-type sonication to ensure the homogeneous dispersion of the f-SWCNT in the SEBS solution. Finally, f-SWCNT-reinforced SEBS films with a thickness of about 0.51 mm were obtained using a solution casting method by removing the residual solvent in a vacuum dryer. Depending on the required SWCNT wt % of the composites, f-SWCNTs were initially dispersed in toluene (10 mL) by sonication at room temperature. These solutions were then combined with SEBS solution in toluene (20 mL) to yield a total composite mass of approximately 2 g. The final product solution was poured onto a glass petri-dish, and the solvent was evaporated at 50°C in a hot air oven to obtain polymer films with a thickness of about 20 μm.

Instrumentation

Raman spectroscopy (LabRam HR Ar-ion laser 514 nm, Longjumeau, France) was used to confirm the functionalization of the SWCNTs. X-ray photoelectron spectroscopy (XPS, ESCSA 2000) was used to analyze the surface composition of the CNTs. The surface morphology of the functionalized SWCNTs was observed via transmission electron microscopy (TEM, JEM 2100F, JEOL, Tokyo, Japan). The dispersion of the SWCNTs in the nanocomposites was analyzed on the basis of surface

Applied Polymer SCIENCE

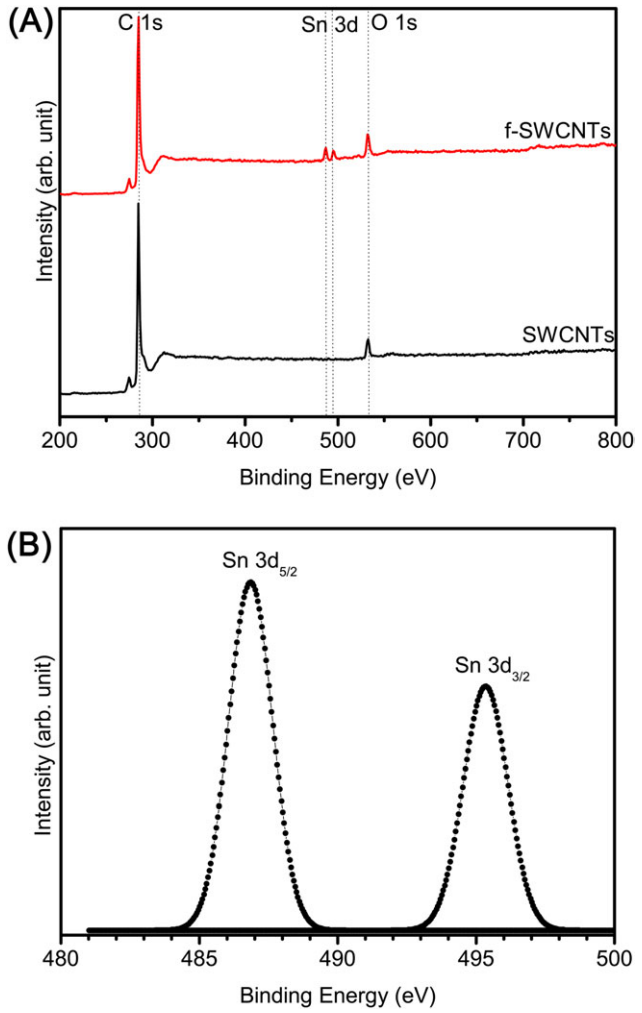

Figure 2. XPS survey scan of SWCNTs and f-SWCNTs (A), and high-resolution XPS Sn (3d) profile of f-SWCNTs (B). [Color figure can be viewed in the online issue, which is available at wileyonlinelibrary.com.]

morphology using a field emission scanning electron microscope (FE-SEM, S-4300SE, Hitachi, Tokyo, Japan). The mechanical properties of the nanocomposites were measured at an elongation rate of 10 mm/min, at room temperature, using a tensile tester (Instron 4468). The dielectric constant and AC electrical conductivity of the samples were measured with a dielectric analyzer (Broadband Dielectric Analyzer, Novocontrol GmbH, Hundsangen, Germany) in the frequency range of 10^1 to 10^6 Hz. Samples were mounted between two gold-plated parallel plates and placed in a sealed cell at atmospheric pressure.

Table I. Relative Atomic Concentration of Carbon and Oxygen in the Pristine and the Noncovalently Functionalized SWCNTs

Atomic concentration	Pristine SWCNTs	f-SWCNTs
Carbon (%)	95.7	94.4
Oxygen (%)	4.3	5.1
Tin (%)	0	0.5
O/C	0.045	0.054
Sp^2/sp^{3a}	4.7	4.8

[a] sp^2/sp^3 is the ratio of the integrated intensity of the sp^2-carbon assigned peak at 285.8 eV relative to the integrated intensity of the sp^3-carbon assigned peak at 284.6 eV.

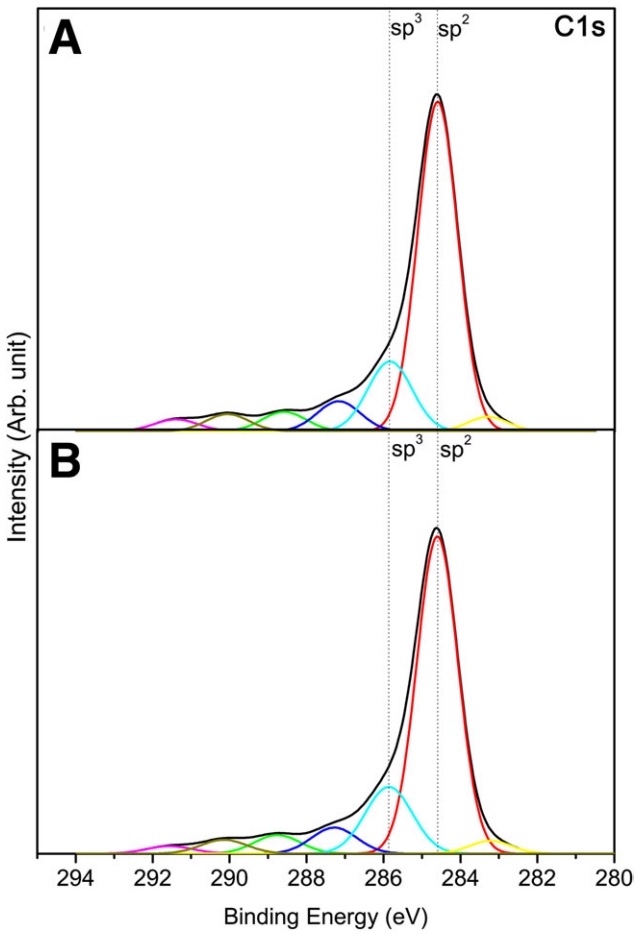

Figure 3. C(1s) high-resolution XPS profile of SWCNTs (A) and f-SWCNTs (B). [Color figure can be viewed in the online issue, which is available at wileyonlinelibrary.com.]

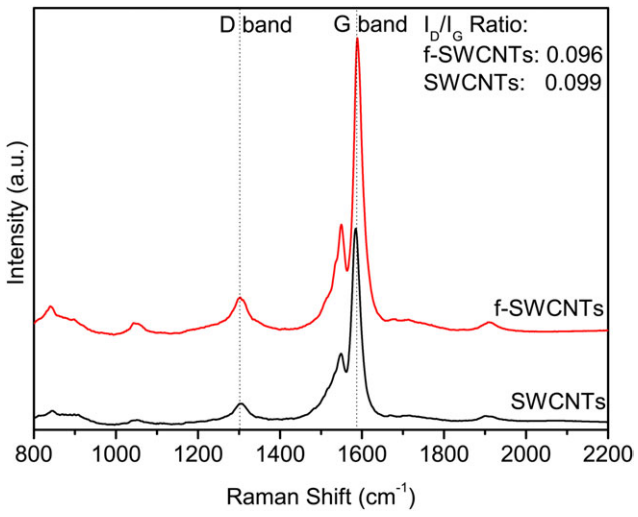

Figure 4. Raman spectra of SWCNTs and f-SWCNTs. [Color figure can be viewed in the online issue, which is available at wileyonlinelibrary.com.]

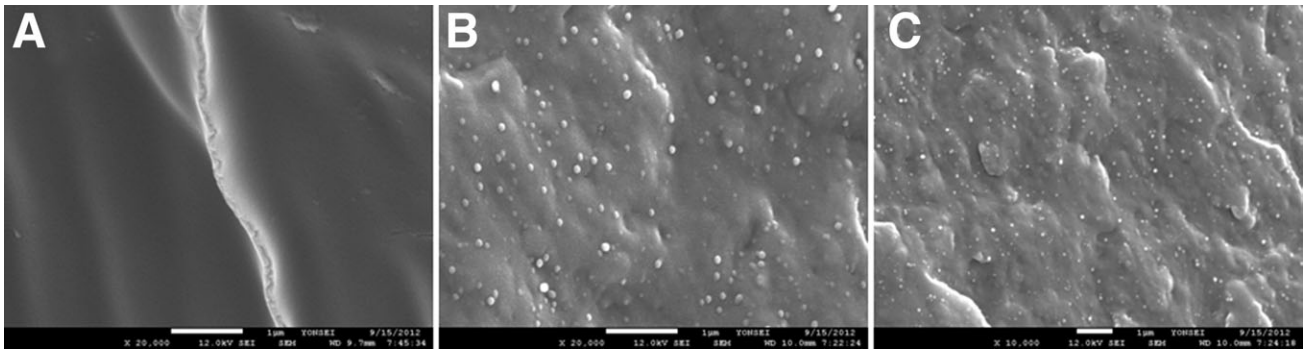

Figure 5. FE-SEM images of (A) pure SEBS, (B) SEBS-f-SWCNT-1.5, and (C) SEBS-f-SWCNT-2.0.

RESULTS AND DISCUSSION

Noncovalent Functionalization of SWCNTs

Functionalization of SWCNTs was performed simply by mixing the SWCNTs with DBTDL at 60°C for 5 h (Scheme 1). To confirm the modification of the surface properties of the SWCNTs resulting from the noncovalent functionalization, Raman, XPS, energy dispersive x-ray analysis (EDX), and TEM measurements were carried out on the pristine SWCNTs and the f-SWCNTs. Figure 1 shows TEM images and the EDX spectrum of the f-SWCNTs. The smooth surface of the f-SWCNT and the Sn peak in the EDX spectrum provide evidence of the presence of DBTDL on the surface of the SWCNTs without any defect formation. XPS was also used to examine the surface of the f-SWCNTs. Figure 2(A) shows the XPS survey spectra of the original SWCNTs and the f-SWCNTs. Two strong peaks at 285.0 eV (C 1s) and 532.6 eV (O 1s) are observed for both samples, and two new, relatively weak signals corresponding to Sn (3d) are also observed at 487.0 and 495.0 eV for the f-SWCNTs. The relative atomic concentration of Sn in the f-SWCNTs was calculated to be 0.5%, confirming the presence of DBTDL on the surface of the f-SWCNTs (Table I). Figure 2(B) displays the high-resolution XPS profile of the Sn 3d region of the f-SWCNTs. The peaks centered at 495.0 and 487.0 eV are attributed to Sn $3d_{3/2}$ and Sn $3d_{5/2}$ levels, respectively, which provide further confirmation of the presence of DBTDL on the surface of the SWCNTs.

The C 1s XPS spectra were also acquired to evaluate which functional groups on the surface of the SWCNTs were subjected to the noncovalent functionalization (Figure 3). The strong peak at 284.6 eV is attributed to the sp^2 bonded carbon atoms, while the broad peak at 285.8 eV arises from the sp^3 bonded carbon atoms (i.e., dangling bonds). Even though there is no ostensible change in the C 1s XPS spectra of the CNTs due to the noncovalent functionalization [Figure 3(B)], it was found that the relative concentration of oxygen atoms was enhanced for the f-SWCNTs. In addition, the intensified peaks corresponding to COOH, —COO, and —C—O— groups at 290.5, 288.6, and 286.7 eV also indicate a substantial introduction of oxygen-containing functional groups on the outer surface of the f-SWCNTs. The peak at 291.3 eV is used to assign the shake-up peak (p–p* transitions).[29]

The relative atomic concentration of oxygen atoms in the f-SWCNTs was calculated to be 5.1%; the enhanced concentration of oxygen further corroborates the presence of the DBTDL on the surface of the f-SWCNTs (Table I). Figure 4 shows the Raman spectra of the pristine and noncovalently functionalized SWCNTs. Two characteristic bands are observed at 1587 cm^{-1} (G band) and 1301 cm^{-1} (D band). The D band corresponds to disordered sp^3 hybridization, whereas the G band indicates the

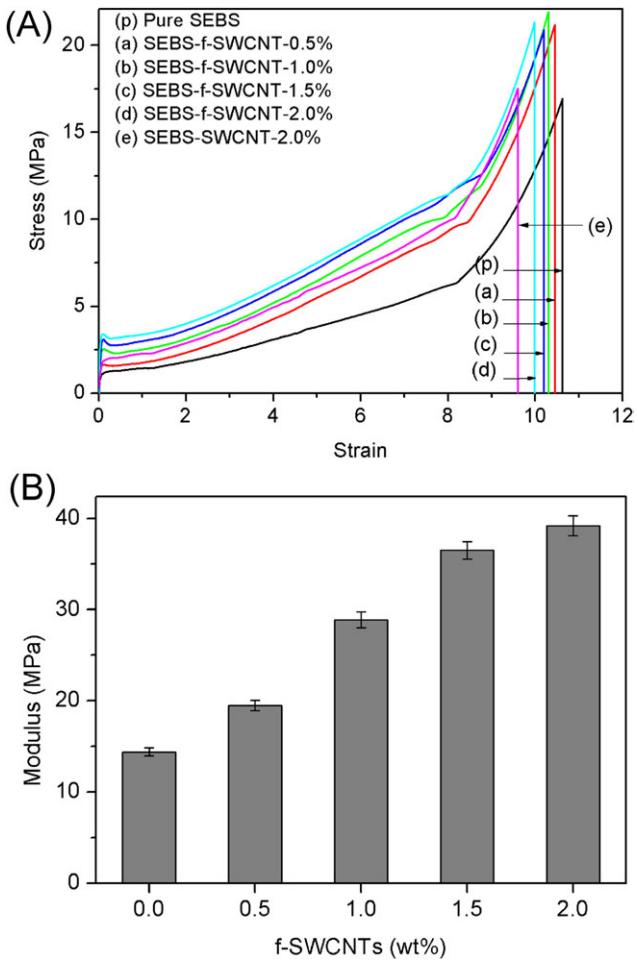

Figure 6. Stress–strain curves (A) and modulus (B) of nanocomposites. [Color figure can be viewed in the online issue, which is available at wileyonlinelibrary.com.]

Table II. Sample Formulation and Mechanical Properties of Nanocomposites

Sample code	SWCNTs (wt %)	Breaking stress (MPa)	Breaking strain (%)	Modulus (MPa)
SEBS	0	16.9 ± 0.89	10.6 ± 0.78	14.4 ± 0.43
SEBS-f-SWCNT-0.5	0.5	21.2 ± 1.3	10.4 ± 0.69	19.5 ± 0.59
SEBS-f-SWCNT-1.0	1.0	21.9 ± 1.9	10.3 ± 0.75	28.9 ± 0.87
SEBS-f-SWCNT-1.5	1.5	20.9 ± 1.5	10.1 ± 0.58	36.5 ± 0.95
SEBS-f-SWCNT-2.0	2.0	21.4 ± 1.8	9.9 ± 0.53	39.2 ± 1.08
SEBS-SWCNT-2.0	2.0	17.5 ± 0.92	9.58 ± 0.82	29.6 ± 0.91

presence of ordered sp^2 hybridization.[30] The intensity ratio (I_D/I_G) values are the same for the pristine SWCNTs and the f-SWCNTs, which suggests that no structural disorder was generated by the attack of DBTDL on the sidewall of the tubes. These data, in conjunction with the previously presented data, prove the successful noncovalent functionalization of the SWCNTs with DBTDL. There may be some physical interaction between DBTDL and the SWCNTs. Figure 5 shows FE-SEM images of the fractured surfaces of the composites, illustrating the even dispersion of the SWCNTs due to functionalization of the MWCNTs.

Mechanical and Dielectric of SEBS-f-SWCNT Nanocomposites

The elasticity of the pure SEBS and SEBS-f-SWCNT composites was evaluated via tensile tests (Figure 6). A dramatic reinforcement of the SEBS matrix is evident in the presence of the added f-SWCNTs, that is, all of the nanocomposites have a higher modulus and greater breaking strength than the neat SEBS. This strengthening effect increases with increasing f-SWCNT loading. Interestingly, all of the nanocomposites show excellent stretchability as evidenced by the very high elongation-at-break.[31] Moreover, only a slight decrease in the elongation-at-break is evident for the nanocomposites with increasing f-SWCNT content, in contrast to most inorganic filler-reinforced polymer composites.[32,33] Figure 6(B) and Table II illustrate the improved modulus and breaking strength of the nanocomposites. For example, the SEBS-f-SWCNT nanocomposites displayed approximately 2.7- and 1.3-fold increases in the modulus and breaking stress, respectively, compared to the pure SEBS. All of the composites retained excellent stretchability, which is a key characteristic of flexible elastomeric materials, even after incorporation of the f-SWCNTs. These results are considered to be due to the rich interface between the f-SWCNTs and SEBS resulting from the noncovalent functionalization. The high dispersion of the SWCNTs within the SEBS films without the formation of aggregated f-SWCNTs is attributed to the same cause, and these characteristics are reflected in the enhanced mechanical properties. However, the composite of pristine SWCNT and SEBS has showed the deterioration of mechanical properties compared to the f-SWCNT-based composites.

Figure 7(A,B) show the dielectric constant and dielectric loss of the SEBS-f-SWCNT composites at room temperature as a function of frequency and of f-SWCNT loading. The inclusion of f-SWCNTs in the SEBS matrix dramatically increased the dielectric constant from 2.1 for pure SEBS to approximately 1000 at 1 Hz for 2 wt % f-SWCNT composites, while still maintaining a relatively low electrical conductivity (Figure 8). Figure 8 demonstrates the frequency dependence of the AC conductivity of the nanocomposites. With increasing f-SWNTs loading, a typical concentration behavior for the electrical conductivity of the nanocomposites was observed. Their electrical conductivity increased with increasing f-WCNT content.

It is, therefore, possible to achieve a much higher dielectric constant using the f-SWCNT-polymer composites than pure SEBS, while still maintaining similar or lower dielectric loss. DBTDL has been used as a catalyst and a stabilizer for polymers. DBTDL contains Sn metal in the center; the current approach

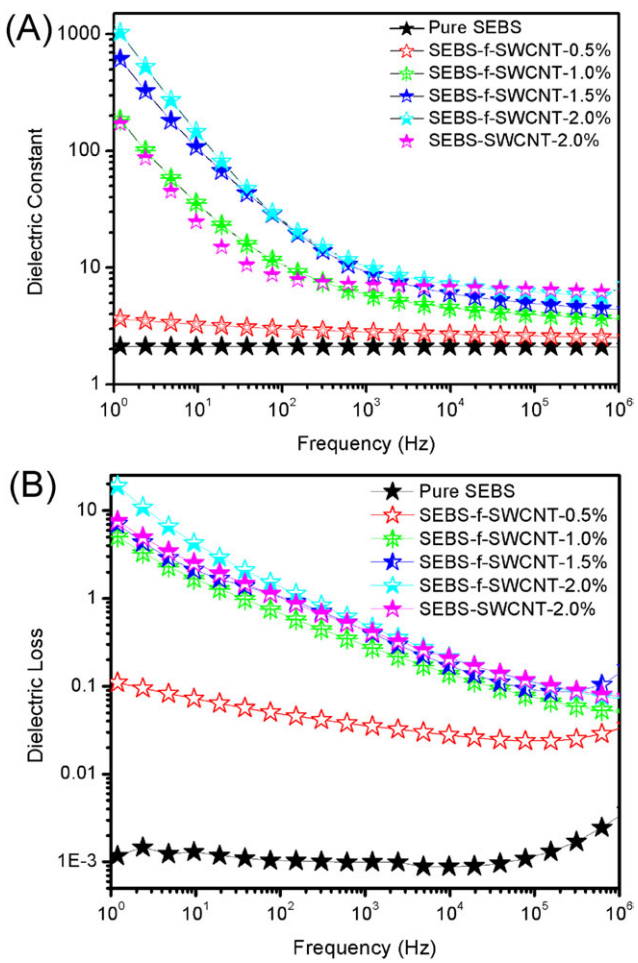

Figure 7. Dielectric constant (A) and dielectric loss (B) of nanocomposites. [Color figure can be viewed in the online issue, which is available at wileyonlinelibrary.com.]

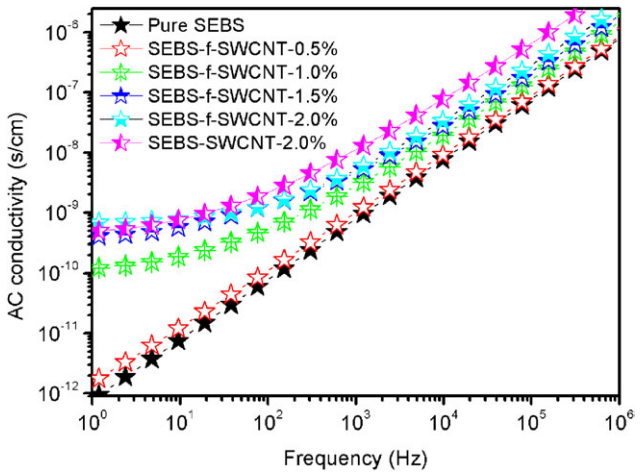

Figure 8. Frequency dependence of AC conductivity of nanocomposites. [Color figure can be viewed in the online issue, which is available at wileyonlinelibrary.com.]

can thus be considered as a kind of metal doping on the SWCNT surfaces.[34] The high dielectric permittivity achieved with this composite may be due to the synergetic effect of the SWCNTs and Sn metal. The large dielectric constant can be explained by a minicapacitor principle. In the composites system, the f-SWCNTs were dispersed in the insulated polymer matrix, which can generate many minicapacitors. The number of the minicapacitors enhanced with increasing concentration of f-SWCNT. The functionalized f-SWCNTs contact with each other, the minicapacitor may be also formed because of the functional groups on the surface of SWCNTs. Due to the large SWCNT concentration and the functional groups on the surface of the SWCNTs, there are more minicapacitors in the composites. The isolation distance between the f-SWCNTs decreases with increasing the filler concentration so that the capacitance of the single minicapacitor increases. Therefore, the different largest dielectric constants of composites can be ascribed to the variation of f-SWCNT concentration.[3,35]

When the f-SWCNT concentrations were equal to or less than 1.5%, as in the case of 0.5, 1.0, and 1.5 wt %, the dielectric loss varied from 0.1 to 8, which can be explained from the perspective of the percolation threshold. The SWCNTs were well dispersed in the insulating SEBS elastomer, and consequently, the CNTs were out of the conducting network. When the concentration of f-SWCNTs is higher as in the case of the 2 wt % sample, the dielectric permittivity and dielectric loss become more pronounced and frequency dependent with increasing concentration. At lower frequencies, both the dielectric constant and dielectric loss achieved high values and then diminish exponentially with the increase in frequency. This behavior clearly indicates that the effect of interfacial polarization becomes more predominant at lower frequency. The decrease in permittivity and loss factor with the increase in frequency can be also explained by the fact that at high frequencies electric field changes too fast for the polarization effects to appear (Figure 7B).[36–46]

CONCLUSION

We have presented a simple and novel route for fabrication of high-dielectric composites containing individually dispersed f-SWCNTs in a SEBS matrix. The individually reinforced f-SWCNTs conferred high dielectric permittivity on the composites with very low dielectric loss, as well as improved mechanical properties due to enhanced nanotube dispersion. The SEBS-f-SWCNT nanocomposites with 2 wt % of f-SWCNT loading displayed approximately 2.7- and 1.3-fold increases in the modulus and breaking stress, respectively, compared to the pure SEBS. The SEBS matrix dramatically increased the dielectric constant from 2.1 for pure SEBS to approximately 1000 at 1 Hz for 2 wt % f-SWCNT composites, while still maintaining a relatively low electrical conductivity. The developed f-SWCNT-reinforced polymer composites may find potential application in electronic devices, artificial muscle materials, and actuators.

ACKNOWLEDGMENTS

This study was supported by the Defense Acquisition Program Administration (DAPA) and the Agency for Defense Development (ADD).

REFERENCES

1. Zhang, Q. M.; Li, H.; Poh, M.; Xia, F.; Cheng, Z. Y.; Xu, H.; Huang, C. *Nature* **2002**, *419*, 284.
2. Maliakal, A.; Katz, H.; Cotts, P. M.; Subramoney, S.; Mirau, P. *J. Am. Chem. Soc.* **2005**, *127*, 14655.
3. Mahapatra, S. S.; Yadav, S. K.; Yoo, H. J.; Cho, J. W. *J. Mater. Chem.* **2011**, *21*, 7686.
4. Stoyanov, H.; Kollosche, M.; McCarthy, D. N.; Kofod, G. *J. Mater. Chem.* **2010**, *20*, 7558.
5. Dang, Z. M.; Wang, L.; Yin, Y.; Zhang, Q.; Lei, Q. Q. *Adv. Mater.* **2007**, *19*, 852.
6. Dang, Z.-M.; Yuan, J.-K.; Zha, J.-W.; Zhou, T.; Li, S.-T.; Hu, G.-H. *Prog. Mater. Sci.* **2012**, *57*, 660.
7. Bai, Y.; Cheng, Z. Y.; Bharti, V.; Xu, H. S.; Zhang, Q. M. *Appl. Phys. Lett.* **2000**, *76*, 3804.
8. Yadav, S. K.; Madeshwaran, S. R.; Cho, J. W. *J. Colloid Interface Sci.* **2011**, *358*, 471.
9. Iijima, S. *Nature* **1991**, *354*, 56.
10. Konidari, M. V.; Soulas, D. N.; Papadokostaki, K. G.; Sanopoulou, M. *J. Appl. Polym. Sci.* **2012**, *125*, E471.
11. Wang, L.; Dang, Z.-M. *Appl. Phys. Lett.* **2005**, *87*, 042903.
12. Yadav, S. K.; Mahapatra, S. S.; Cho, J. W.; Lee, J. Y. *J. Phys. Chem. C* **2010**, *114*, 11395.
13. Sahoo, N. G.; Rana, S.; Cho, J. W.; Li, L.; Chan, S. H. *Prog. Polym. Sci.* **2010**, *35*, 837.
14. Yadav, S. K.; Mahapatra, S. S.; Cho, J. W. *Polymer* **2012**, *53*, 2023.
15. Bose, S.; Khare, R. A.; Moldenaers, P. *Polymer* **2010**, *51*, 975.
16. Price, B. K.; Lomeda, J. R.; Tour, J. M. *Chem. Mater.* **2009**, *21*, 3917.

17. Romanos, G. E.; Likodimos, V.; Marques, R. R. N.; Steriotis, T. A.; Papageorgiou, S. K.; Faria, J. L.; Figueiredo, J. L.; Silva, A. N. M. T.; Falaras, P. *J. Phys. Chem. C* **2011**, *115*, 8534.
18. Nasiri, A.; Shariaty-Niasar, M.; Rashidi, A.; Amrollahi, A.; Khodafarin, R. *Exp. Therm. Fluid Sci.* **2010**, *35*, 717.
19. Lucente-Schultz, R. M.; Moore, V. C.; Leonard, A. D.; Price, B. K.; Kosynkin, D. V.; Lu, M.; Partha, R.; Conyers, J. L.; Tour, J. M. *J. Am. Chem. Soc.* **2009**, *131*, 3934.
20. Chen, R. J.; Zhang, Y.; Wang, D.; Dai, H. *J. Am. Chem. Soc.* **2001**, *123*, 3838.
21. Kang, Y.; Taton, T. A. *J. Am. Chem. Soc.* **2003**, *125*, 5650.
22. Dang, Z.-M.; Yao, S.-H.; Yuan, J.-K.; Bai, J. *J. Phys. Chem. C* **2010**, *114*, 13204.
23. Yang, C.; Lin, Y.; Nan, C.W. *Carbon* **2009**, *47*, 1096.
24. Kohlmeyer, R. R.; Javadi, A.; Pradhan, B.; Pilla, S.; Setyowati, K.; Chen, J.; Gong, S. *J. Phys. Chem. C* **2009**, *113*, 17626.
25. Lipert, R. J.; Shinar, R.; Vaidya, B.; Pris, A. D.; Porter, M. D.; Liu, G.; Grabau, T. D.; Dilger, J. P. *Anal. Chem.* **2002**, *74*, 6383.
26. Ranade, S. V.; Richard, R. E.; Helmus, M. N. *Acta Biomater.* **2005**, *1*, 137.
27. Shankar, R.; Krishnan, A. K.; Ghosh, T. K.; Spontak, R. J. *Macromolecules* **2008**, *41*, 6100.
28. Leu, Y. Y.; Mohd Ishak, Z. A.; Chow, W. S. *J. Appl. Polym. Sci.* **2012**, *124*, 1200.
29. Ramos, S. C.; Lobo, A. O.; de Vasconcelos, G.; Antunes, E. F.; Trava-Airoldi, V. J.; Corat, E. J. *Theor. Chem. Acc.* **2011**, *130*, 1061.
30. Yadav, S. K.; Mahapatra, S. S.; Yoo, H. J.; Cho, J. W. *Nanoscale Res. Lett.* **2011**, *6*, 122.
31. Li, Y.; Shimizu, H. *Macromolecules* **2009**, *42*, 2587.
32. Yadav, S. K.; Yoo, H. J.; Cho, J. W. *J. Polym. Sci. Part B: Polym. Phys.* **2013**, *51*, 39.
33. Yadav, S. K. J.; Cho, J. W. *Appl. Surf. Sci.* **2013**; DOI: 10.1016/j.apsusc.2012.12.028
34. Yu, H.; Li, S.; Zhong, J.; Xu, K. *J. Appl. Polym. Sci.* **2006**, *99*, 1986.
35. Li, Q.; Xue, Q.; Hao L.; Gao, X.; Zheng, Q. *Compos. Sci. Technol.* **2008**, *68*, 2290.
36. Sohi, N. J .S.; Rahaman, M.; Khastgir, D. *Polym. Compos.* **2011**, *32*, 1148.
37. Pérez, R. *J. Appl. Polym. Sci.* **2009**, *113*, 2264.
38. Nayak, L.; Chaki, T. K.; Rahaman, M.; Khastgir, D. *Polym. Bull.* **2011**, *67*, 1038.
39. Dang, Z.-M.; Fan, L.-Z.; Shen, Y.; Nan, C.-W. *Mater. Sci. Eng. B* **2003**, *103*, 140.
40. Magioli, M.; Soares, B. G.; Sirqueira, A. S.; Rahaman, M.; Khastgir, D. *J. Appl. Polym. Sci.* **2012**, *125*, 1476.
41. Nogales, A.; Broza, G.; Roslaniec, Z.; Schulte, K.; Sÿics, I.; Hsiao, B. S.; Sanz, A.; GarcõÂa-GutieÂrrez, M. C.; Rueda, D. R.; Domingo, C.; Ezquerra, T. A. *Macromolecules* **2004**, *37*, 7669.
42. Thomas, P. S.; Abdullateef, A. A.; Al-Harthi, M. A.; Atieh, M. A.; De, S. K.; Rahaman, R.; Chaki, T. K., Khastgir, D.; Bandyopadhyay, S. *J. Mater. Sci.* **2012**, *47*, 3344.
43. Clayton, L. M.; Sikder, A. K.; Kumar, A.; Cinke, M.; Meyyappan, M.; Gerasimov, T. G.; Harmon, J. P. *Adv. Funct. Mater.* **2005**, *15*, 101.
44. Rahaman, M.; Chaki, T. K.; Khastgir, D. *J. Appl. Polym. Sci.* **2012**; DOI: 10.1002/APP.38137.
45. Wang, L.; Danga, Z. M. *Appl. Phys. Lett.* **2005**, *87*, 042903.
46. Rahaman, M.; Chaki, T. K.; Khastgir, D. *J. Mater. Sci.* **2012**, *46*, 3989.